Bright photon upconversion on organic lanthanide molecules through localized thermal radiation

Huanqing Ye[#], Viktor Bogdanov[#], Sheng Liu[#], Saumitra Vajandar[†], Thomas Osipowicz[†], Ignacio Hernández[‡], Qihua Xiong[#‖╪]

[#]Division of Physics and Applied Physics, School of Physical and Mathematical Sciences, Nanyang Technological University, 21 Nanyang Link, 637371, Singapore.

[†]Centre for Ion Beam Applications, Department of Physics, Faculty of Science, National University of Singapore, 2 Science Drive 3, 117542, Singapore.

[‡]Dpto. CITIMAC, Facultad de Ciencias, Universidad de Cantabria, Avda. Los Castros, s/n 39005 Santander, Spain.

[‖]NOVITAS, Nanoelectronics Center of Excellence, School of Electrical and Electronic Engineering, Nanyang Technological University, 639798, Singapore.

[╪]MajuLab, CNRS-UNS-NUS-NTU International Joint Research Unit, UMI 3654, Singapore.

AUTHOR INFORMATION

Corresponding Author

*Prof Qihua Xiong; E-mail: qihua@ntu.edu.sg

ABSTRACT: Converting low-energy photons via thermal radiation can be a potential approach to utilize IR photons to improve photovoltaic efficiency. Lanthanide-containing materials have achieved great progress in IR to visible photon upconversion (UC). Herein, we firstly report bright photon, tunable wavelength UC through localized thermal radiation at the

molecular scale with low excitation power density (< 10 W/cm^2) realized on lanthanide complexes of perfluorinated organic ligands. This is enabled by engineering the pathways of nonradiative de-excitation and energy transfer in a mixture of ytterbium and terbium perfluoroimidodiphosphinates. The IR excited thermal UC and wavelength control is realized through the terbium activators sensitized by the ytterbium sensitizers of having high luminescence efficiency. The metallic molecular complexes can be potential energy material in the use of IR solar spectrum for thermal photovoltaic applications.

TOC GRAPHICS

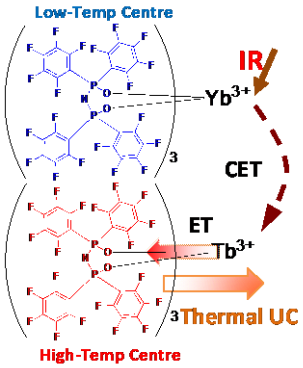

KEYWORDS: photon upconversion, thermal radiation, perfluorinated organic lanthanide molecules

The solar spectrum contains a large portion of IR photons that are below the bandgap of most photovoltaic (PV) semiconductor materials. Thus, they cannot be absorbed by a single-junction PV device. Converting IR photons to visible photons of which the energies are above the PV material bandgap would be a solution.[1,2] Lanthanide based materials are mostly used for photon UC through excited state absorption (ESA) or energy transfer upconversion (ETU).[3,4] ETU is termed as cooperative energy transfer (CET) if simultaneous sensitization is achieved in one activator from two sensitizers.[5–7] However, the problems of weak lanthanide absorption and weakly-doped concentration only give weak UC brightness. Thermal radiation

induced photon UC has been recently demonstrated in weakly lanthanide doped inorganic oxides as a bright alternative.[8,9] This mechanism is that the IR absorption that heats the materials through nonradiative multiphonon relaxation results in substantial thermal (black-body type) radiation. Then, the extracted high-energy photons are emitted in a range that can be absorbed by commercial PV devices, potentially delivering cost-effective thermal PV devices to exceed the efficiency limit.[10,11] However, the nonradiative process is negligible in lanthanide based inorganics with long lanthanide emission lifetimes of a few milliseconds, which requires high excitation power density over 200 W/cm^2.[8] For eliminating thermal loss, low thermal conductivity of the inorganics must be used but the material choices are quite limited, and the bulk crystals have to be cracked,[8,9,12] implying difficulty in developing them into realistic thermal PV devices.

Organic lanthanide materials would have specific features: Organic lanthanide molecules reduce the ion trapping centers, thus increasing the doped concentration; Intense organic ligand vibrations, which in fact prevent typically any use in UC-related applications, provide diverse nonradiative relaxation channels to deexcite the lanthanide excitations.[13,14] Organic materials usually have lower thermal conductivity <1 W/(m-K) than many oxides.[15] These interplay among them make it is interesting to consider organic lanthanide materials as a possibility in obtaining high-energy photons through thermal UC. However, difficulties will arise in the control of nonradiative channels, material stability, wavelength control, etc.

Herein we firstly realize bright photon UC on organic lanthanide molecules through thermal and photoluminescence (PL) emission processes. We demonstrate that NIR-emitting ytterbium (Yb) sensitizers that are chelated with perfluorinated organic ligands and the internal quantum yield (IQY) of Yb PL approaching unity cause terbium (Tb)-based molecules activators to incandesce brightly in the visible without significant losses. Moreover, the existence of a superimposed Tb UC permits a channel to further control the emission wavelength.

We have chosen tetrakis(pentafluorophenyl)imidodiphosphinimidic (F-TPIP$^-$) ligand (L$^-$) to obtain Yb, Tb and Y complexes that are vacuum compatible to make integrated optic devices and can be incorporated in mixture systems. The detailed material related information can be found in Supporting Information (SI). In Figure 1a, the pristine YbL_3 absorption merely gives the peak at 975 nm wavelength corresponds to the Yb $^2F_{7/2} \rightarrow 2F_{5/2}$ transition with no organic ligand absorption observed in the region. PL consists an emission band from 780 to 1150 nm wavelengths, where the 780 to 830 nm wavelengths region shows the tail of the anti-Stokes emission of $^2F_{5/2} \rightarrow {}^2F_{7/2}$ transition. Ligand shielding of Yb ions barely differs the complex absorption in solution and solid. Thus, we take the absorption spectrum in DMSO to calculate the radiative lifetime (τ_{rad}) of the Yb emission, which gives the τ_{rad}(solid) = 1.0 ± 0.2 ms taking into account the difference of refractive index[16] and the uncertainty of estimating the refractive index in solid (Section 4, SI).

The PL decay trace for the thin film placed in air, shown in Figure 1b, gives a Yb emission lifetime $\tau_{Yb(air)}$ = 0.56 ± 0.03 ms. However, the film placed in vacuum (< 10^{-2} mbar) exhibits a long PL lifetime of 1.10 ± 0.06 ms (Figure S6, SI). We ascribe the difference to the trapped trace H_2O molecules in air, which are capable of permeating the space between the molecules (Figure 1c) through the small depth (20 nm) of the molecular grains observed in the morphological arrangement of the film. The result implies that the trace H_2O molecules of being not coordinated with the central ions are significant quenching centres for Yb emission. However, we find they desorb in vacuum, which facilely prevents this quenching. Moreover, this ~ 1.1 ms lifetime is found to be sustainable with the Yb concentration diluted by optically inactive yttrium (Y) units in the series of $[YbL_3]_x[YL_3]_{1-x}$ (x = 0.7, 0.5, 0.1) (inset to Figure 1b). The unchanged lifetimes indicate that the Yb concentration quenching is very much reduced in the concentrated compound. We believe the reason is that the ligand shell isolates Yb ions from any quenching trap due to Yb ion concentration.[17,18]

The acquisition of the radiative lifetime and the PL lifetime gives a direct measurement of the internal quantum yield (IQY) of Yb emission. Given this we estimate IQY = τ_{Yb}/τ_{rad} within the experimental error with a value approaching unity (>50% in air, >86% in vacuum). The high IQY implies that direct vibrational quenching by the organic ligands is reduced. This elimination can be rationalized regarding the low phonon energies in the perfluorinated complex, and no evident vibration frequencies or overtones detected > 1650 cm^{-1} in the FTIR spectrum of the complex (Figure S3, SI).

To harvest Yb IR excitations, we chose the Tb ion as the activator. This choice is critical to realize bright UC because the Tb ion has no intermediate energy levels from the $^7F_{0\text{-}7}$ levels (< 5000 cm^{-1}) to the $^5D_4$ level (~ 20000 cm^{-1}) and their energy gap ($\Delta E \geq 15{,}000$ cm^{-1}) widely exceeds the F-TPIP$^-$ vibrational energies (> 1650 cm^{-1}), while the intermediate ΔE among $^7F_{0\text{-}7}$ levels are well resonant with the organic vibrational energies. We employ $[YbL_3]_{0.7}[TbL_3]_{0.3}$, where the mixture ratio giving a Yb/Tb ratio of 2, which was reported to provide the most efficient CET UC in Yb-Tb mixed system.[6, 7] CET induced Tb-based UC takes place with continuous-wave (CW) 975 nm excitation when the complex powder in vacuum (Figure S7, SI), allowed by the long Yb excited state lifetime.

We then use high vacuum (~10^{-5} mbar) to further eliminate the permeated gas molecules, particularly trace H_2O and N_2, to reduce the thermal loss in the materials. This method turns effective since Figure 2a shows a bright thermal UC for the sample in high vacuum, while the brightness decreases with the vacuum decreased. In high vacuum, the visible fraction rises when CW 975 nm excitation power increases from 2.5 to 10.0 W/cm^2 and gradually overwhelms the Tb UC (left inset to Figure 2a). Corresponding blackbody temperature (T_{BB}) can be obtained using the emission region (450 to 800 nm) by Planck's law fit, and the power dependence of the laser-induced T_{BB} is shown in Figure 2b. We found T_{BB} increases up to ~ 1300 K at 10 W/cm^2, while the T_{BB} and the spectral radiance (Sr) intensity start to drop after ~ 12.0 W/cm^2 due to the rapid material decomposition or evaporation.

Interestingly, the spectrum in the IR region from 1010 to 1300 nm wavelengths primarily exhibits the Yb emission of being much more intense than the IR fraction of the thermal radiation. Integrating Yb emission from 1010 to 1200 nm with the thermal radiation background subtracted remains roughly linear with power during the heating (right inset to Figure 2a) on a logscale power dependence plot. This linearity allows using differential luminescence thermometry (DLT)[19] (Figure S8, SI) to estimate the average temperature (T_{Ave}) of YbL_3 molecules, shown in Figure 2c, only increased to a lower temperature of ~ 382 K within 0.3 to 10 W/cm^2. Replacing Tb with Y shows negligible thermal radiation in $[YbL_3]_{0.7}[YL_3]_{0.3}$ within higher excitation power (> 7.8 W/cm^2) in Figure 2b, and the Sr is at least 2 orders of the magnitude weaker than one for the $[YbL_3]_{0.7}[TbL_3]_{0.3}$ thermal UC at the same laser excitation level (Figure S9, SI). Suppressed laser-induced heating on YbL_3 units and lower T_{Ave} can be expected due to the evidence of the eliminated nonradiative de-excitation directly from the Yb to organics. These evidence also make us believe that the thermal UC is localized on TbL_3 molecules of being the key to reducing the excitation power of < 10 W/cm^2, one order of magnitude lower than the reported excitation power for the thermal UC in inorganic oxides and comparable to the conventional lanthanide-based UC.[8,20,21] Low excitation power implies less solar concentration technology is required.

Figure 3 shows the time evolution of the dynamics and the energy migration routes. Yb PL decay trace in $[YbL_3]_{0.7}[TbL_3]_{0.3}$ of being 0.79 ± 0.06 ms lifetime (5 ns pulse excitation) in vacuum becomes shorter than the pristine lifetime $\tau_{YbY(IR)}$ of ~ 1.1 ms, giving a CET rate is estimated to be $\tau_{Yb\rightarrow Tb(UC)}^{-1} = \tau_{YbTb(IR)}^{-1} - \tau_{YbY(IR)}^{-1} \approx 356\ s^{-1}$. Tb 550 nm emission peak shows a lifetime of 1.32 ± 0.07 ms (Figure 3) with the direct excitation (5 ns pulse excitation) into the Tb $^5D_4$ level, while Tb 550 nm UC (inset to Figure 3) shows a slightly shorter lifetime of 1.22 ± 0.07 ms with quasi-CW (38 ms square pulse) 975 nm excitation in vacuum. This might be due to the phonon-assisted energy migration between Tb ions enhanced by the laser-induced

heating. Particularly, the inter-ion interaction for the Tb ions could be dominant since the Tb emission lifetime is shorter than the reported one for TbL_3 dissolved in deuterated solvents.[22] The thermal UC has a longer rise time (20 ms ~ 45 ms) (Figure S10, SI) than one for Tb UC, which implies the thermal dissipation from beforehand-excited Tb units to Yb units to heat the materials to T_{Ave}. Nevertheless, it is likely that the thermal dissipation among molecular clusters is disrupted due to the ~ 20 nm vacuum space between grains, which could reduce the thermal loss from the high-temperature centers to the neighboring ones. This might explain the rise time being much shorter than those (from seconds to minutes) in crystalline or nanocrystalline oxides, which have higher thermal conductivity benefiting thermal dissipation over bulky hosts.[9,12] Our discovered phenomena thus are distinct from the thermal UC in lanthanide doped inorganics, in which the sensitizers and host have no temperature difference.

According to the literature method,[8] we can estimate the emission quantum efficiency (QE) for the process, QE = 0.13% at 975 nm excitation with 10W/cm^2 from the ratio of the integrated band radiance to the integrated spectral radiance. Our thermal UC QE is limited by the maximum reachable blackbody temperature that is lower than ~2100K reached in inorganics.[8,9] However, the low excitation power can give a comparable normalized QE of 1.33×10^{-4} cm^2/W at 1300 K to those achieved in the UC of inorganics.[8] The stability of the organic materials containing aromatic rings up to the ~1200 K has been reported even in the hydrogenated metallic complex such as copper phthalocyanine in vacuum.[23,24] Also, perfluorinated materials are known to have much higher thermal stability in general.[25,26] In our studied complexes, the overall effect of the coordinated perfluorinated aromatic rings of –(C6F5), the ring configuration of –(O-P-N-P-O)– and the high geometric symmetry of the complex molecule[27] could further enhance the thermal stability. In fact, investigating the time-stability of the thermal radiation in $[YbL_3]_{0.7}[TbL_3]_{0.3}$ indicates the unchanged chemical composition of the material at the available level of detection (details in Section 8, SI).

We have unprecedentedly realized the bright photon UC on organic lanthanide molecules in the solid state by engineering the dynamic pathways among the Yb sensitizers, Tb activators and organic ligands. The temperature difference in the mixture is firstly demonstrated, owning to the ultra-high IQY of Yb emission in pristine Yb perfluorinated complex. The results imply a new approach allowing for improved convenience and compatibility for integrating such energy material system as a photon UC layer onto thermal PV devices.

EXPERIMENTAL METHODS

Details of experimental methods in material synthesis, optical characterisaion, and data analysis are available in SI. In summary, tetrakis(pentafluorophenyl)-imidodiphosphinate acid (> 98% Changzhou Garde Pharmtech Co. Ltd, China), and the lanthanide chlorides (> 99.99% Sigma-Aldrich) are commercially purchased. Materials are purified using vacuum train purification in prior to the use for experiments. Film samples are fabricated using high-vacuum deposition system. $\boldsymbol{B(\lambda, T_{\mathrm{BB}})} = \left(\frac{\boldsymbol{2h^2}}{\boldsymbol{\lambda^5}}\right)\left(\boldsymbol{e^{\frac{hc}{\lambda k_B T}} - 1}\right)$ according to Planck's law was used to fit thermal radiation spectra to yield T_{BB} with $R^2 > 0.99$. Exponential functions were used for lifetime fitting. A home-made vacuum chamber was used to place the materials in vacuum.

ASSOCIATED CONTENT

Supporting Information is available from the Wiley Online Library or from the author.

ACKNOWLEDGMENT

Q.X. acknowledges the support from the Singapore National Research Foundation through Investigatorship award (NRF-NRFI2015-03), and the Singapore Ministry of Education via an AcRF Tier 2 grant (MOE2013-T2-1-049) and a Tier1 grant (2015-T1-001-175). IH acknowledges EU FP7 (MC-CIG Grant 303535) and Spanish MINECO (Grant MAT2016-80438-P).

REFERENCES

(1) Wang, H.; Batentschuk, M.; Osvet, A.; Pinna, L.; Brabec, C. J. Rare-Earth Ion Doped Up-Conversion Materials for Photovoltaic Applications. *Adv. Mater.* **2011**, *23* (22-23), 2675–2680.

(2) Yu, M.; Qu, Y.; Pan, K.; Wang, G.; Li, Y. Enhanced Photoelectric Conversion Efficiency of Dye-Sensitized Solar Cells by the Synergetic Effect of $NaYF_4:Er^{3+}/Yb^{3+}$ and G-C_3N_4. *Sci. China Mater.* **2017**, *60* (3), 228–238.

(3) Haase, M.; Schäfer, H. Upconverting Nanoparticles. *Angew. Chemie Int. Ed.* **2011**, *50* (26), 5808–5829.

(4) Gargas, D. J.; Chan, E. M.; Ostrowski, A. D.; Aloni, S.; Altoe, M. V. P.; Barnard, E. S.; Sanii, B.; Urban, J. J.; Milliron, D. J.; Cohen, B. E. Engineering Bright Sub-10-Nm Upconverting Nanocrystals for Single-Molecule Imaging. *Nat. Nanotechnol.* **2014**, *9* (4), 300–305.

(5) Salley, G. M.; Valiente, R.; Güdel, H. U. Cooperative $Yb^{3+}-Tb^{3+}$ Dimer Excitations and Upconversion in $Cs_3Tb_2Br_9$: Yb^{3+}. *Phys. Rev. B* **2003**, *67* (13), 134111.

(6) Hernández, I.; Pathumakanthar, N.; Wyatt, P. B.; Gillin, W. P. Cooperative Infrared to Visible Up Conversion in Tb^{3+}, Eu^{3+}, and Yb^{3+} Containing Polymers. *Adv. Mater.* **2010**, *22* (47), 5356–5360.

(7) Souri, N.; Tian, P.; Platas-Iglesias, C.; Wong, K.-L.; Nonat, A.; Charbonnière, L. J. Upconverted Photosensitization of Tb Visible Emission by NIR Yb Excitation in Discrete Supramolecular Heteropolynuclear Complexes. *J. Am. Chem. Soc.* **2017**, *139* (4), 1456–1459.

(8) Wang, J.; Ming, T.; Jin, Z.; Wang, J.; Sun, L.-D.; Yan, C.-H. Photon Energy Upconversion through Thermal Radiation with the Power Efficiency Reaching 16%. *Nat. Commun.* **2014**, *5*.

(9) Soares, M. R. N.; Ferro, M.; Costa, F. M.; Monteiro, T. Upconversion Luminescence and Blackbody Radiation in Tetragonal YSZ Co-Doped with Tm^{3+} and Yb^{3+}. *Nanoscale* **2015**, *7* (47), 19958–19969.

(10) Bierman, D. M.; Lenert, A.; Chan, W. R.; Bhatia, B.; Celanović, I.; Soljačić, M.; Wang, E. N. Enhanced Photovoltaic Energy Conversion Using Thermally Based Spectral Shaping. *Nat. Energy* **2016**, *1*, 16068.

(11) Boriskina, S. V; Chen, G. Exceeding the Solar Cell Shockley–Queisser Limit via Thermal up-Conversion of Low-Energy Photons. *Opt. Commun.* **2014**, *314*, 71–78.

(12) Chen, Z.; Jia, H.; Sharafudeen, K.; Dai, W.; Liu, Y.; Dong, G.; Qiu, J. Up-Conversion Luminescence from Single Vanadate through Blackbody Radiation Harvesting Broadband near-Infrared Photons for Photovoltaic Cells. *J. Alloys Compd.* **2016**, *663*, 204–210.

(13) Bünzli, J.-C. G. On the Design of Highly Luminescent Lanthanide Complexes. *Coord. Chem. Rev.* **2015**, *293–294*, 19–47.

(14) Tan, R. H. C.; Motevalli, M.; Abrahams, I.; Wyatt, P. B.; Gillin, W. P. Quenching of IR Luminescence of Erbium, Neodymium, and Ytterbium β-Diketonate Complexes by Ligand CH and CD Bonds. *J. Phys. Chem. B* **2006**, *110* (48), 24476–24479.

(15) Kim, N.; Domercq, B.; Yoo, S.; Christensen, A.; Kippelen, B.; Graham, S. Thermal Transport Properties of Thin Films of Small Molecule Organic Semiconductors. *Appl. Phys. Lett.* **2005**, *87*, 24.

(16) Shavaleev, N. M.; Scopelliti, R.; Gumy, F.; Bünzli, J.-C. G. Surprisingly Bright Near-Infrared Luminescence and Short Radiative Lifetimes of Ytterbium in Hetero-Binuclear Yb−Na Chelates. *Inorg. Chem.* **2009**, *48* (16), 7937–7946.

(17) Johnson, N. J. J.; He, S.; Diao, S.; Chan, E. M.; Dai, H.; Almutairi, A. Direct Evidence for Coupled Surface and Concentration Quenching Dynamics in Lanthanide-Doped Nanocrystals. *J. Am. Chem. Soc.* **2017**, *139* (8), 3275–3282.

(18) Hernández, I.; Zheng, Y.-X.; Motevalli, M.; Tan, R. H. C.; Gillin, W. P.; Wyatt, P. B. Efficient Sensitized Emission in Yb (III) Pentachlorotropolonate Complexes. *Chem. Commun.* **2013**, *49* (19), 1933–1935.

(19) Seletskiy, D. V; Melgaard, S. D.; Bigotta, S.; Di Lieto, A.; Tonelli, M.; Sheik-Bahae, M. Laser Cooling of Solids to Cryogenic Temperatures. *Nat. Photonics* **2010**, *4* (3), 161–164.

(20) Hyppänen, I.; Lahtinen, S.; Ääritalo, T.; Mäkelä, J.; Kankare, J.; Soukka, T. Photon Upconversion in a Molecular Lanthanide Complex in Anhydrous Solution at Room Temperature. *ACS Photonics* **2014**, *1* (5), 394–397.

(21) Suffren, Y.; Golesorkhi, B.; Zare, D.; Guénée, L.; Nozary, H.; Eliseeva, S. V; Petoud, S.; Hauser, A.; Piguet, C. Taming Lanthanide-Centered Upconversion at the Molecular Level. *Inorg. Chem.* **2016**.

(22) Glover, P. B.; Bassett, A. P.; Nockemann, P.; Kariuki, B. M.; Van Deun, R.; Pikramenou, Z. Fully Fluorinated Imidodiphosphinate Shells for Visible-and NIR-Emitting Lanthanides: Hitherto Unexpected Effects of Sensitizer Fluorination on Lanthanide Emission Properties. *Chem. Eur. J.* **2007**, *13* (22), 6308–6320.

(23) ERK, P.; HENGELSBERG, H. 119 - Phthalocyanine Dyes and Pigments. In *The Porphyrin Handbook*; Kadish, K. M., Smith, K. M., Guilard, R., Eds.; Academic Press: Amsterdam, 2003; pp 105–149.

(24) Lawton, E. A. The Thermal Stability of Copper Phthalocyanine. *J. Phys. Chem.* **1958**, *62* (3), 384.

(25) Johns, I. B.; McElhill, E. A.; Smith, J. O. Thermal Stability of Organic Compounds. *Ind. Eng. Chem. Prod. Res. Dev.* **1962**, *1* (1), 2–6.

(26) Johns, I. B.; McElhill, E. A.; Smith, J. O. Thermal Stability of Some Organic Compounds. *J. Chem. Eng. Data* **1962**, *7* (2), 277–281.

(27) Ye, H.-Q.; Peng, Y.; Li, Z.; Wang, C.-C.; Zheng, Y.-X.; Motevalli, M.; Wyatt, P. B.; Gillin, W. P.; Hernández, I. Effect of Fluorination on the Radiative Properties of Er^{3+} Organic Complexes: An Opto-Structural Correlation Study. *J. Phys. Chem. C* **2013**, *117* (45), 23970–23975.

FIGURES AND CAPTIONS

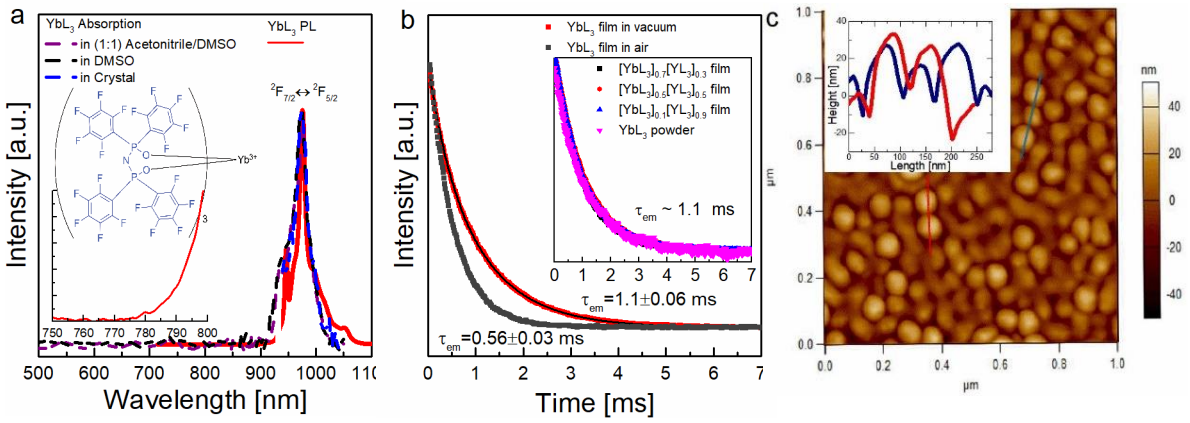

Figure 1. **a**, Absorption in solution and solid, and PL spectrum for YbL_3 powder, where L is F-TPIP. The wavelength region from 940 nm to 1050 nm was recorded at 910 nm excitation. The wavelength region from 700 to 900 nm shows the onset of Yb anti-Stokes emission at 975 nm excitation. **b**, Time dependence of Yb PL using a 5 ns pulse at 975 nm excitation. The red dots for YbL_3 film emission in vacuum and the black solid is the fitting curve with a single exponential function (details in SI). The grey dots represent the spectrum data for the film emission exposed in air. The inset displays the corresponding Yb emission decays for $[YbL_3]_x[YL_3]_{1-x}$ (x = 0.1, 0.5, 0.7) films and YbL_3 powder. **c**, AFM topography of a 200 nm thick $[YbL_3]_x[YL_3]_{1-x}$ film surface on a sapphire substrate in a 1×1 μm^2 area.

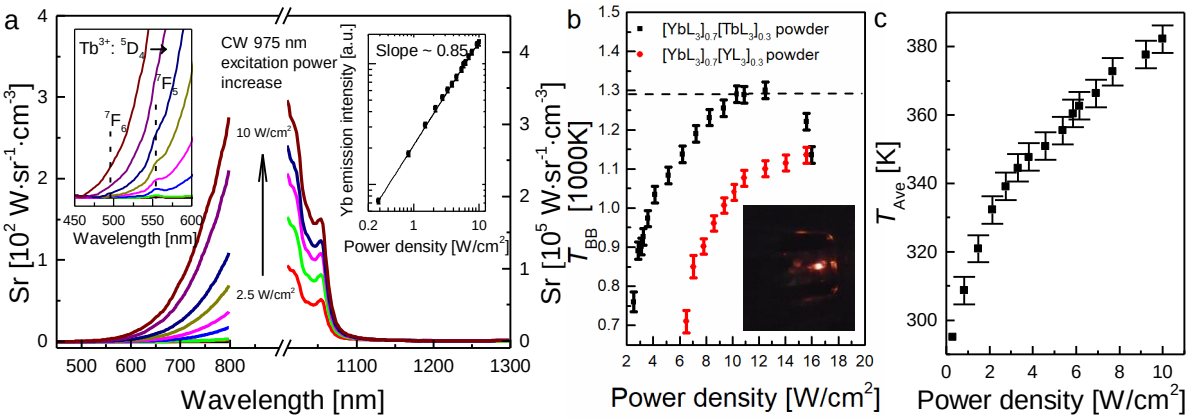

282

283 **Figure 2**. **a**, Emission of $[YbL_3]_{0.7}[TbL_3]_{0.3}$ powder at 10^{-5} mbar vacuum taken at CW 975 nm

284 excitation, where L is F-TPIP. The visible region (450 to 800 nm) primarily exhibits the

285 visible fraction of the thermal radiation with the Tb emission peaks (Tb^{3+} $^5D_4 \rightarrow {}^7F_{6,5}$) (zoom

286 in, left inset). The NIR region (1010 to 1300 nm) primarily exhibits the conventional

287 ytterbium emission. The power dependence of the integrated ytterbium emission intensities is

288 plotted with logarithmic scale shown in the right inset. b, Power dependence of the fitted T_{BB}

289 for the thermal radiation after 975 nm excitation for $[YbL_3]_{0.7}[TbL_3]_{0.3}$ powder (black dots)

290 and $[YbL_3]_{0.7}[YL_3]_{0.3}$ powder (red dots). The error bar is of ± 20 K. The inset shows a picture

291 of the visible fraction of the thermal radiation with 10 W/cm^2. The powder was mounted into

292 a glass tube in a vacuum chamber. A 950 nm short-pass filter was employed to filter off laser

293 scattering. c, Estimated T_{Ave} of YbL_3 molecules in $[YbL_3]_{0.7}[TbL_3]_{0.3}$ mixture system, derived

294 from differential luminescence thermometry with an error bar of ± 5K.

295

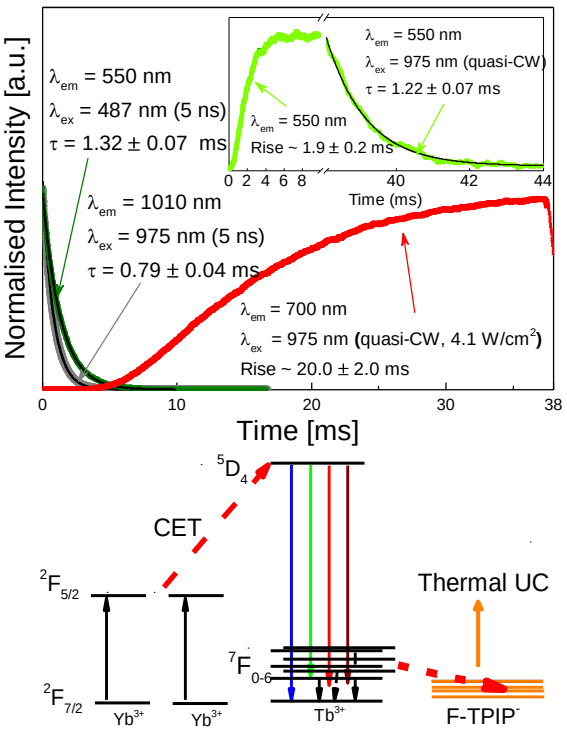

Figure 3. Time evolution of photon emission in in $[YbL_3]_{0.7}[TbL_3]_{0.3}$ powder: Yb PL (grey dots) for 975 nm excitation using a 5.0 ns pulse. Tb^{3+}:$^5D_4 \rightarrow {}^7F_5$ emission (dark green dots) when directly excited to $^5D_4$ level using a 5 ns pulse at 487 nm excitation. Tb^{3+}:$^5D_4 \rightarrow {}^7F_5$ emission (green dots, the inset) when excited using a square 38.0 ms pulse at 975 nm excitation. Fitting curves (black lines) are using single exponential functions (details in SI). The thermal UC recorded at 700 nm wavelength (red curve) when excited using a square 38.0 ms pulse at 975 nm excitation. The time values resulted from the fit of the exponential functions. Jablonski diagram (below) detailing the energy transfer processes among Yb, Tb and organic vibrations. Dashed arrows represent non-radiative processes and coloured solid arrows represent the absorption and emission of photons, respectively; The red dashed arrows represent the CET from Yb^{3+}:$^2F_{5/2}$ to Tb^{3+}:$^5D_4$, and multiphonon-relaxation from Tb to organic vibrations. The black dashed arrows represent nonradiative deactivations in Tb^{3+} transitions.